

This is the accepted manuscript made available via CHORUS. The article has been published as:

Phonon and magnon excitations in block-antiferromagnetic $\text{K}_{0.88}\text{Fe}_{1.63}\text{S}_2$

N. Lazarević, Hechang Lei (✉), C. Petrovic, and Z. V. Popović

Phys. Rev. B **84**, 214305 — Published 12 December 2011

DOI: [10.1103/PhysRevB.84.214305](https://doi.org/10.1103/PhysRevB.84.214305)

Phonon and magnon excitations in block-antiferromagnetic $\text{K}_{0.88}\text{Fe}_{1.63}\text{S}_2$

N. Lazarević,¹ Hechang Lei (雷和畅),² C. Petrovic,² and Z. V. Popović¹

¹*Center for Solid State Physics and New Materials,
Institute of Physics Belgrade, University of Belgrade,
Pregrevica 118, 11080 Belgrade, Serbia*

²*Condensed Matter Physics and Materials Science Department,
Brookhaven National Laboratory, Upton, NY 11973, USA*

(Dated: November 28, 2011)

The vibrational properties of $\text{K}_{0.88}\text{Fe}_{1.63}\text{S}_2$ were investigated using Raman spectroscopy and analyzed on the basis of peculiarities of its crystal structure. Fourteen Raman active modes, predicted by factor-group analysis, were observed and assigned, confirming Fe vacancy ordering. Phonon energy temperature dependance is fully driven by anharmonicity effects in the range of 80-300 K. High energy Raman spectra revealed two-magnon excitations of three optical magnon branches. It is shown that magnetic structure of this material is consistent with the high temperature block-antiferromagnetism of $\text{K}_{0.8}\text{Fe}_{1.6}\text{Se}_2$.

PACS numbers: 78.30.-j; 71.28.+d; 75.30.Ds; 75.50.Pp

I. INTRODUCTION

The discovery of superconductivity in iron-based layered materials¹ with T_c up to 55 K, has attracted a lot of attention in recent years. The proximity and coexistence of superconductivity and antiferromagnetic phase in $\text{A}_x\text{Fe}_{2-y}\text{S}_2$ ($\text{A} = \text{K}, \text{Rb}, \text{Cs}$ and Tl) materials (AFSe-122 type) might imply that magnetic fluctuations play an important role in understanding of the pairing mechanism.²⁻⁴ On the other hand, the absence of strong magnetic fluctuations in ^{77}Se NMR and the presence of static magnetic order with $T_N \sim 500$ K⁵ suggest sample and/or stoichiometry dependent magnetic phase that arises due to intrinsic nanoscale phase separation.⁶⁻¹⁰ The properties of these materials are closely related to the vacancy ordering in the two-dimensional Fe-atom square lattice.^{11,12}

Very recently, the discovery of $\text{K}_x\text{Fe}_{2-y}\text{S}_2$ single crystals isostructural to 122 iron selenide superconductors has been reported.¹³ $\text{K}_x\text{Fe}_{2-y}\text{S}_2$ exhibits similar vacancy order on both potassium and iron site as its selenide counterpart. The resistivity measurements¹³ demonstrated semiconductor behavior. Detailed magnetic measurements on $\text{K}_{0.88}\text{Fe}_{1.63}\text{S}_2$ single crystals suggest spin glass transition below about 33 K, similar to TlFe_xSe_2 ,¹⁴ and a possible magnetic order above the room temperature.

Raman scattering was used to determine the influence of vacancy ordering on phonon and magnon spectra of $\text{K}_{0.88}\text{Fe}_{1.63}\text{S}_2$ single crystals. Fourteen Raman active modes were successfully observed and assigned according to their symmetry. Analysis of the temperature dependence of Raman scattering spectra showed that the Raman active phonon energies in the range of 80-300 K are fully driven by anharmonicity effects without any signatures of electron-phonon interaction. Raman spectra of $\text{K}_{0.88}\text{Fe}_{1.63}\text{S}_2$ at energies higher than the optical phonon range revealed existence of two-magnon excitations. Magnetic structure of this material is very similar

to the block-antiferromagnetism of $\text{K}_{0.8}\text{Fe}_{1.6}\text{Se}_2$ and in agreement with the theoretical predictions.

II. EXPERIMENT

Single crystals of $\text{K}_{0.88}\text{Fe}_{1.63}\text{S}_2$ were grown and characterized as described elsewhere in detail.¹³ The samples were cleaved in order to obtain a flat, shiny (001)-plane surface. Freshly-cleaved crystal was put into the cryostat within 30 s, and evacuated to 10^{-6} mbar. The sample was orientated so that one of the principle axis is parallel to the analyzer polarization orientation. The Raman scattering measurements were performed using TriVista 557 Raman system in backscattering micro-Raman configuration. The 514.5 nm line of an Ar^+/Kr^+ mixed gas laser was used as an excitation source. Focusing of the laser beam was realized with a long distance microscope objective (magnification $50\times$). We have found that laser power level of 0.04 mW on the sample is sufficient to obtain Raman signal and, except signal to noise ratio, no changes of the spectra were observed as a consequence of laser heating by further lowering laser power. The corresponding excitation power density was less then 0.2 kW/cm^2 . Low temperature measurements were performed between 80 K and 300 K using KONTI CryoVac continuous Helium flow cryostat with 0.5 mm thick window.

III. RESULTS AND DISCUSSION

Hypothetical KFe_2S_2 (the ThCr_2Si_2 -type of crystal structure) crystallizes in tetragonal structure of the $\text{I}_{4/mmm}$ space group (D_{4h}^{17} , $Z^B = 1$).¹⁵ The real unit cell of $\text{K}_x\text{Fe}_{2-y}\text{S}_2$ is built up of interspersed puckered FeS slabs and nets of K, stacked along the c axis (see Fig. 1). Because of FeS and K layers distortion the sym-

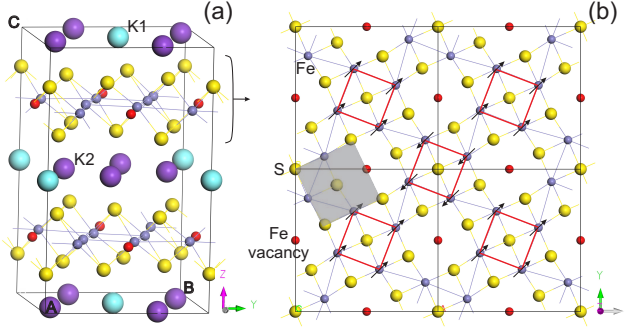


FIG. 1. (Color online) (a) Crystal structure of $K_{0.8}Fe_{1.6}S_2$ in $I_{4/m}$ unit cell (black lines). Fe1 (red balls) represent iron vacant sites. (b) FeS slab in (001) plane with ordered iron vacancies. Red lines represent ferromagnetic ordered blocks. These blocks form a block-checkerboard antiferromagnetic pattern. Grey square illustrate $I_{4/mmm}$ unit cell.

metry is reduced to the $I_{4/m}$ (C_{4h}^5) space group with $Z^B=5$ (Fig. 1).¹³ The ordering pattern of Fe vacancies is the same as in $K_xFe_{2-y}Se_2$.² When both Fe and K vacancy are completely ordered, Fe1 and K1 sites are fully unoccupied, whereas K2 and Fe2 are fully occupied with corresponding chemical formula $K_{0.8}Fe_{1.6}S_2$. All site symmetries and corresponding occupancies for the non-stoichiometric $K_{0.88}Fe_{1.63}S_2$ sample are presented in Table I.

By using correlation method we were able to obtain each site contribution to the normal mode distribution at the center of the Brillouin zone for both ideal 122 and non-stoichiometric compound (Table I). According to this representation, in the Raman scattering experiment one can expect a total of 25 Raman-active modes for the $K_{0.88}Fe_{1.63}S_2$ and only four Raman active modes for the KFe_2S_2 . We have used the (001) plane of $K_{0.88}Fe_{1.63}S_2$ single crystals for Raman scattering measurements. Therefore, only the A_g and B_g symmetry modes can be observed in our experimental configuration, in which both incident and scattered light are polarized parallel to the (001) crystal plane (see Table I). If the vacancies were not ordered, only two Raman active modes ($A_{1g}+B_{1g}$) should be observed.

Fig.2(a) shows Raman scattering spectra of $K_{0.88}Fe_{1.63}S_2$ single crystals measured at 100 K in crossed and parallel polarization configuration. There are at least seven peaks which can be observed in both parallel and crossed polarization configuration. The number of the observed peaks is much larger than the number of Raman active modes predicted for $I_{4/mmm}$ symmetry. This confirms vacancy order and crystallographic space group symmetry lowering to $I_{4/m}$. According to selection rules for C_{4h} symmetry (Table I), the B_g symmetry modes can be observed in both polarization configurations. In order to separate the A_g from the B_g symmetry modes we have performed Raman scattering measurements for different angles between polarizations of incident and scattered light

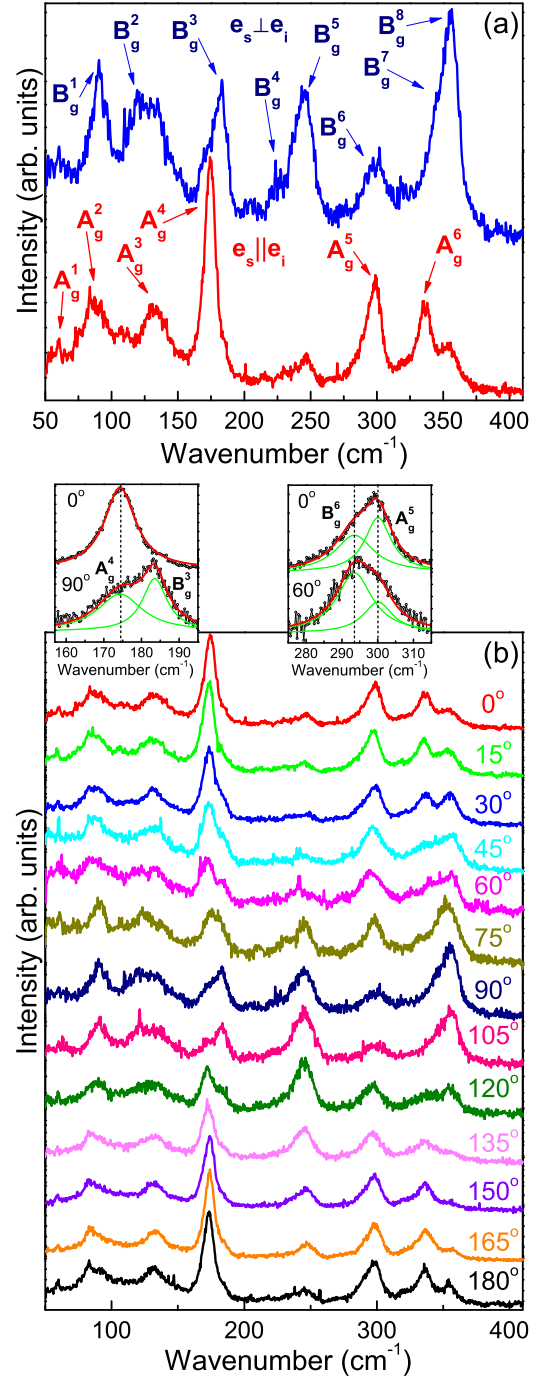


FIG. 2. (Color online) Raman scattering spectra of $K_{0.88}Fe_{1.63}S_2$ single crystals measured at 100 K (a) in cross and parallel polarization configuration and (b) as a function of $\Theta = \angle(\vec{e}_s, \vec{e}_i)$.

$$(\Theta = \angle(\vec{e}_s, \vec{e}_i)).$$

Fig. 2(b) presents Raman scattering spectra of $K_{0.88}Fe_{1.63}S_2$ single crystals measured at 100 K as a function of angle Θ . Closer inspection of the angle-dependent Raman spectra revealed that most of the observed peaks are actually doublets of different symmetry (A_g and B_g)

TABLE I. Top panel gives the type of atoms, their site symmetries, Raman tensors and selection rules for KFe_2S_2 . Bottom panel gives the type of atoms, occupancy, and their site symmetries for $\text{K}_{0.88}\text{Fe}_{1.63}\text{S}_2$. The irreducible representations of the phonon modes, Raman tensors, activity, selection rules as well as experimentally obtained values at 100 K for A_g and B_g modes.

KFe ₂ S ₂ (D ¹⁷ _{4h} and Z ^B =1)			
Atoms	Occupancy	Site symmetry	Irreducible representations
K	1	D _{4h}	A _{2u} +E _u
Fe	1	D _{2d}	A _{2u} +B _{1g} +E _g +E _u
S	1	C _{4v}	A _{1g} +A _{2u} +E _g +E _u
Raman tensors			
A _{1g} = $\begin{pmatrix} a & 0 & 0 \\ 0 & a & 0 \\ 0 & 0 & b \end{pmatrix}$	B _{1g} = $\begin{pmatrix} c & 0 & 0 \\ 0 & -c & 0 \\ 0 & 0 & 0 \end{pmatrix}$	E _g = $\begin{pmatrix} 0 & 0 & -e \\ 0 & 0 & 0 \\ -e & 0 & 0 \end{pmatrix}$	E _g = $\begin{pmatrix} 0 & 0 & 0 \\ 0 & 0 & e \\ 0 & e & 0 \end{pmatrix}$
Activity and selection rules			
Γ _{Raman} =A _{1g} (α _{xx+yy} , α _{zz})+B _{1g} (α _{xx-yy})+2E _g (α _{xz} , α _{yz})		Γ _{infrared} =2A _{2u} (E z)+2E _u (E x , E y)	
Γ _{acoustic} =A _u +E _u			
K _{0.88} Fe _{1.63} S ₂ (C ⁵ _{4h} and Z ^B =5)			
Atoms	Occupancy ¹³	Site symmetry	Irreducible representations
K1	0.84	C _{4h}	A _u +E _u
K2	0.89	C _s	2A _g +A _u +2B _g +B _u +E _g +2E _u
Fe1	0.08	S ₄	A _u +B _g +E _g +E _u
Fe2	1	C ₁	3A _g +3A _u +3B _g +3B _u +3E _g +3E _u
S1	1	C ₄	A _g +A _u +E _g +E _u
S2	1	C ₁	3A _g +3A _u +3B _g +3B _u +3E _g +3E _u
Raman tensors			
A _g = $\begin{pmatrix} a & 0 & 0 \\ 0 & a & 0 \\ 0 & 0 & b \end{pmatrix}$	B _g = $\begin{pmatrix} c & d & 0 \\ d & -c & 0 \\ 0 & 0 & 0 \end{pmatrix}$	E _g = $\begin{pmatrix} 0 & 0 & e \\ 0 & 0 & f \\ e & f & 0 \end{pmatrix}$	E _g = $\begin{pmatrix} 0 & 0 & -f \\ 0 & 0 & e \\ -f & e & 0 \end{pmatrix}$
Activity and selection rules			
Γ _{Raman} =9A _g (α _{xx+yy} , α _{zz})+8B _g (α _{xx-yy} , α _{xy})+8E _g (α _{xz} , α _{yz})		Γ _{infrared} =8A _u (E z)+7B _u (<i>silent</i>)+9E _u (E x , E y)	
Γ _{acoustic} =A _u +E _u			
Symmetry	Exp. (cm ⁻¹)	Symmetry	Exp. (cm ⁻¹)
A ¹ _g	60.3	B ¹ _g	89.8
A ² _g	84.0	B ² _g	119.3
A ³ _g	131.7	B ³ _g	183.6
A ⁴ _g	174.7	B ⁴ _g	227.0
A ⁵ _g	300.1	B ⁵ _g	247.2
A ⁶ _g	336.2	B ⁶ _g	183.5
		B ⁷ _g	344.0
		B ⁸ _g	356.2

modes, as illustrated in the insets of Fig. 2 on the example of the 175 and 300 cm^{-1} peaks. All modes clearly display a four-fold symmetry whereas there are two distinguishable groups of modes with different direction of intensity changes with Θ . By comparison with the corresponding Raman tensors, we assign the group that reaches maximum intensity at $\Theta=0^\circ$ as the A_g symmetry, and the other group as the B_g symmetry modes. We have observed and assigned in total six A_g and eight B_g modes. Table I summarizes $\text{K}_{0.88}\text{Fe}_{1.63}\text{S}_2$ Raman mode symmetries and related energies.

Raman spectra of $\text{K}_{0.88}\text{Fe}_{1.63}\text{S}_2$ measured at different temperatures are shown in Fig. 3 (a). Raman mode energies vs temperature dependence for the highest intensity modes are shown in Fig.3 (b)-(j). Solid lines in Fig.3 (b)-(j) represent calculated phonon mode temperature change due to the anharmonicity effects taking into account only three-phonon processes¹⁶

$$\Omega(T) = \Omega_0 - C \left(1 + \frac{2}{e^x - 1} \right), \quad (1)$$

where Ω_0 is the temperature independent contributions

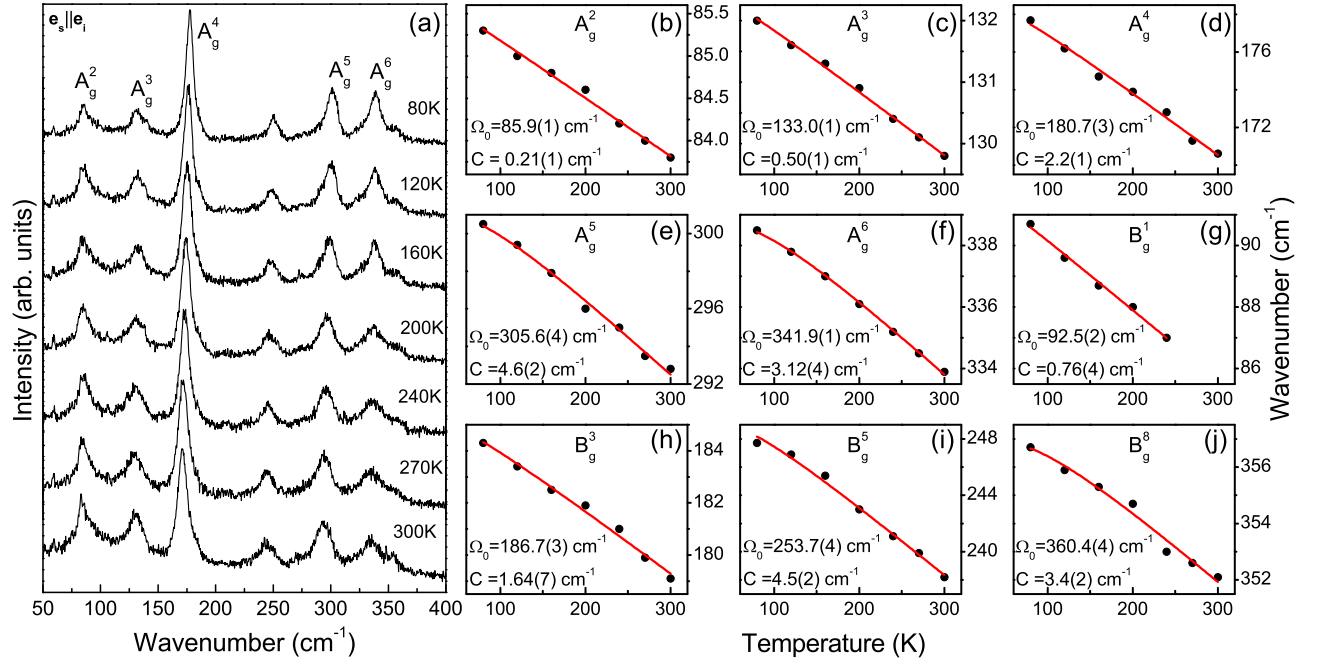


FIG. 3. (Color online) (a) Raman scattering spectra of $K_{0.88}Fe_{1.63}S_2$ single crystals measured in parallel polarization configuration at different temperatures. (b)-(j) Energy of the Raman active phonons of $K_{0.88}Fe_{1.63}S_2$ as a function of temperature. Solid lines represent calculated spectra using Eq. (1).

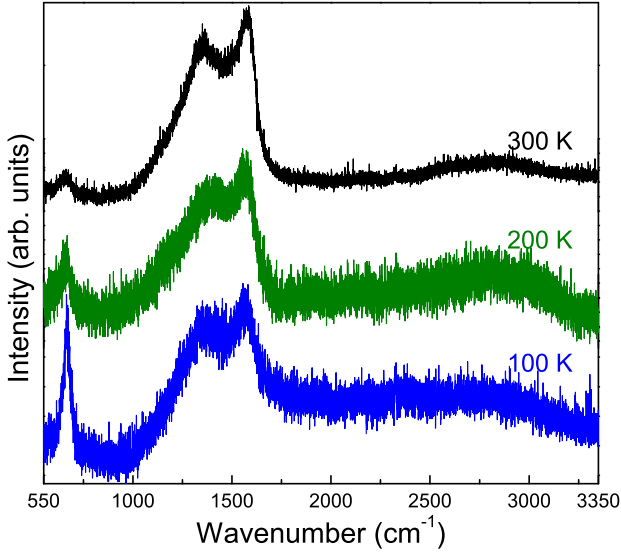


FIG. 4. (Color online) Unpolarized wide range Raman scattering spectra of $K_{0.88}Fe_{1.63}S_2$ single crystals measured at different temperatures.

to the Raman mode energy, C is the anharmonic constant and $x = \hbar\Omega_0/2k_B T$. Excellent agreement between measured and calculated phonon mode temperature dependence suggests absence of any additional temperature dependent couplings in this temperature region.

The ordering pattern of Fe vacancies in $K_{0.88}Fe_{1.63}S_2$ is the same as in $K_xFe_{2-y}Se_2$.¹³ This may imply similar ori-

gin of magnetic behavior for both compounds. It is reasonable to assume that in analogy to $K_xFe_{2-y}Se_2$,^{17–19} the magnetic moments of the four iron atoms in each unit cell align ferromagnetically, along the crystalline c -axis (see Fig. 1). These blocks are staggered from cell to cell to form block-checkerboard antiferromagnetism. If we take that each iron has $S = 2$, one can generally expect eight phonon branches, one doubly degenerate (slightly gapped in the presence of spin anisotropy) acoustic magnon mode and three double degenerate gapped optical magnon modes. The presence of the optical magnon modes is the direct consequence of block antiferromagnetism. It is typical for antiferromagnets that two-magnon Raman scattering is more intense than one-magnon scattering. Contrary to the one-magnon Raman scattering, where contribution comes only from the zone-center magnons, two-magnon scattering contribution comes from magnon pairs from the entire Brillouin zone, and therefore it is expected that the two-magnon spectra spreads over a band of energies. Since the main contribution comes from the zone boundary magnons where the magnon density is the highest, the two-magnon band usually peaks at the energies twice higher than those of the zone boundary magnons.

The $K_{0.88}Fe_{1.63}S_2$ Raman spectra measured in the range between 500 and 3400 cm^{-1} at various temperatures are shown in Fig. 4. The most remarkable feature is the appearance of the broad asymmetric band with two distinguishable peaks at 1345 and 1575 cm^{-1} . The characteristic lineshape of these structures allow us to unequivocally attribute them to the optical two-magnon

excitations. Very broad band at 2800 cm^{-1} can be also attributed to the two-magnon scattering. Recent theoretical investigations of $\text{K}_{0.8}\text{Fe}_{1.6}\text{Se}_2$ predict the existence of three twofold optical magnon branches.^{17,20,21} First two optical magnon branches are degenerate in the Brillouin zone center. Outside the Γ point degeneracy is lifted giving two twofold optical magnon branches at the zone edge. Consequently, one can expect the appearance of a broad band with two peaks. This is in full agreement with the observed picture. The remaining magnon branch is double degenerate in every point of the Brillouin zone and is expected to be found in the higher energy region with the pronounced gap, again in accordance with our findings. We have not observed any remarkable changes in the optical two magnon energies in the temperature region 100-300 K, probably because this system is already at room temperature in the antiferromagnetic state.

Whereas the origin of the peaks at 1345, 1575 and 2800 cm^{-1} is undoubtedly magnetic, the origin of the peak at 660 cm^{-1} remains unclear. This peak falls into the region of two phonon processes and could be two phonon or combinational line mode related.

A very recent inelastic neutron scattering study of $\text{Rb}_{0.89}\text{Fe}_{1.58}\text{Se}_2$ ²² revealed the same pattern of spin excitation as we have observed in $\text{K}_{0.88}\text{Fe}_{1.63}\text{S}_2$. Wang *et al.* have found that spin waves exist in three separate energy ranges: the acoustic magnon branch which starts from 9 meV and extends up to 70 meV, two somewhat flat optical branches from 80 meV to 140 meV, and a high-lying optical branch from 180 meV to 230 meV.

IV. CONCLUSION

We have measured Raman scattering spectra of $\text{K}_{0.88}\text{Fe}_{1.63}\text{S}_2$ single crystal. Fourteen Raman active modes, predicted by factor-group analysis, were successfully observed and assigned. The Raman active phonon energies temperature dependance in the range of 80-300 K is fully driven by anharmonicity effects. Wide range Raman spectra revealed existence of two-magnon excitations. Three optical magnon modes were identified. It is shown that magnetic structure of this material is very similar to the block-antiferromagnetism of $\text{K}_{0.8}\text{Fe}_{1.6}\text{Se}_2$ and $\text{Rb}_{0.89}\text{Fe}_{1.58}\text{Se}_2$.

ACKNOWLEDGMENT

Authors express their thanks to dr Maja Šćepanović for help in measuring Raman spectra. This work was supported by the Serbian Ministry of Education and Science under Projects ON171032 and III45018. Work at Brookhaven is supported by the US Department of Energy (DOE) under Contract No. DE-AC02-98CH10886 and in part by the Center for Emergent Superconductivity, an Energy Frontier Research Center funded by the DOE Office for Basic Energy Science.

-
- ¹ Y. Kamihara, T. Watanabe, M. Hirano, and H. Hosono, *J. Am. Chem. Soc.* **130**, 3296 (2008).
 - ² B. Wei, H. Qing-Zhen, C. Gen-Fu, M. A. Green, W. Du-Ming, H. Jun-Bao, and Q. Yi-Ming, *Chinese Physics Letters* **28**, 086104 (2011).
 - ³ G. M. Zhang, Z. Y. Lu, and T. Xiang, *Phys. Rev. B* **84**, 052502 (2011).
 - ⁴ F. Ye, S. Chi, W. Bao, X. F. Wang, J. J. Ying, X. H. Chen, H. D. Wang, C. H. Dong, and M. Fang, *Phys. Rev. Lett.* **107**, 137003 (2011).
 - ⁵ B. Wei, H. Qing-Zhen, C. Gen-Fu, M. A. Green, W. Du-Ming, H. Jun-Bao, and Q. Yi-Ming, *Chinese Physics Letters* **28**, 086104 (2011).
 - ⁶ D. A. Torchetti, M. Fu, D. C. Christensen, K. J. Nelson, T. Imai, H. C. Lei, and C. Petrovic, *Phys. Rev. B* **83**, 104508 (2011).
 - ⁷ W. Yu, L. Ma, J. B. He, D. M. Wang, T.-L. Xia, G. F. Chen, and W. Bao, *Phys. Rev. Lett.* **106**, 197001 (2011).
 - ⁸ Z. Wang, Y. J. Song, H. L. Shi, Z. W. Wang, Z. Chen, H. F. Tian, G. F. Chen, J. G. Guo, H. X. Yang, and J. Q. Li, *Phys. Rev. B* **83**, 140505 (2011).
 - ⁹ A. Ricci, N. Poccia, G. Campi, B. Joseph, G. Arrighetti, L. Barba, M. Reynolds, M. Burghammer, H. Takeya, Y. Mizuguchi, Y. Takano, M. Colapietro, N. L. Saini, and A. Bianconi, *ArXiv e-prints* (2011), arXiv:1107.0412 [cond-mat.supr-con].
 - ¹⁰ V. Ksenofontov, G. Wortmann, S. Medvedev, V. Tsurkan, J. Deisenhofer, A. Loidl, and C. Felser, *ArXiv e-prints* (2011), arXiv:1108.3006 [cond-mat.supr-con].
 - ¹¹ P. Zavalij, W. Bao, X. F. Wang, J. J. Ying, X. H. Chen, D. M. Wang, J. B. He, X. Q. Wang, G. F. Chen, P.-Y. Hsieh, Q. Huang, and M. A. Green, *Phys. Rev. B* **83**, 132509 (2011).
 - ¹² D. M. Wang, J. B. He, T.-L. Xia, and G. F. Chen, *Phys. Rev. B* **83**, 132502 (2011).
 - ¹³ H. Lei, M. Abeykoon, E. S. Bozin, and C. Petrovic, *Phys. Rev. B* **83**, 180503 (2011).
 - ¹⁴ J. J. Ying, A. F. Wang, Z. J. Xiang, X. G. Luo, R. H. Liu, X. F. Wang, Y. J. Yan, M. Zhang, G. J. Ye, P. Cheng, and X. H. Chen, *ArXiv e-prints* (2010), arXiv:1012.2929 [cond-mat.str-el].
 - ¹⁵ I. R. Shein and A. L. Ivanovskii, *ArXiv e-prints* (2011), arXiv:1102.4173 [cond-mat.supr-con].
 - ¹⁶ M. Balkanski, R. F. Wallis, and E. Haro, *Phys. Rev. B* **28**, 1928 (1983).
 - ¹⁷ C. Cao and J. Dai, *Phys. Rev. Lett.* **107**, 056401 (2011).
 - ¹⁸ X.-W. Yan, M. Gao, Z.-Y. Lu, and T. Xiang, *Phys. Rev. B* **83**, 233205 (2011).
 - ¹⁹ W. Bao, G. N. Li, Q. Huang, G. F. Chen, J. B. He, M. A. Green, Y. Qiu, D. M. Wang, and J. L. Luo, *ArXiv e-prints* (2011), arXiv:1102.3674 [cond-mat.str-el].
 - ²⁰ Y.-Z. You, H. Yao, and D.-H. Lee, *Phys. Rev. B* **84**, 020406 (2011).
 - ²¹ F. Lu and X. Dai, *ArXiv e-prints* (2011), arXiv:1103.5521 [cond-mat.str-el].
 - ²² M. Wang, C. Fang, D.-X. Yao, G. Tan, L. W. Harriger, Y. Song, T. Netherton, C. Zhang, M. Wang, M. B. Stone, W. Tian, J. Hu, and P. Dai, *ArXiv e-prints* (2011), arXiv:1105.4675 [cond-mat.supr-con].